3D anatomy of the Cretaceous–Paleogene age Nadir Crater

Uisdean Nicholson [1] ✉, William Powell[2], Sean Gulick [3,4], Thomas Kenkmann[5], Veronica J. Bray [6], Debora Duarte [1] & Gareth S. Collins [7]

The Nadir Crater offshore West Africa is a recently proposed near K-Pg impact structure identified on 2D seismic. Here we present 3D seismic data that image this crater in exceptional detail, unique for any such structure, which demonstrates beyond reasonable doubt that the crater-forming mechanism was a hypervelocity impact. Seismic mapping reveals a near-circular crater rim of 9.2 km and an outer brim of ~23 km diameter defined by concentric normal faults. An extended damage zone is evident across the region, well beyond the perceived limit of subsurface deformation for impact craters, except in a 'sheltered zone' to the east. The paleo-seabed shows evidence for widespread liquefaction because of seismic shaking, and scars and gullies formed by tsunami wave propagation and resurge. Deformation within the ~425 m high stratigraphic uplift and annular moat allows us to reconstruct the evolution of the crater, with radial thrusts at the periphery of the uplift suggesting a low-angle impact from the east. Structural relationships are used to reconstruct the deformation processes during the crater modification stage, with the central uplift forming first, followed by centripetal flow of surrounding sediments into the evacuated crater floor in the seconds to minutes after impact.

Hypervelocity impacts of large asteroids and comets represent an existential threat to life on Earth[1,2]. Impactors with diameters larger than ~100 m are typically able to penetrate the atmosphere and strike Earth's surface to form a single crater, with impactors of a few 100 m and larger likely representing important regional hazards[2,3]. Despite the hazard that such events represent, empirical evidence for the consequences of hypervelocity impact is limited by the paucity of well-preserved craters on Earth. There are currently only ~200 confirmed impact craters in the terrestrial record[4–7]. Of these, the majority are complex craters, which display a central uplift, collapsed crater rim and annular moat below the crater floor. The formation of central uplifts requires rock to behave in a weaker, more fluid-like manner than expected based on laboratory rock strengths. As crater morphology is ultimately retained, this weakening process is required to be transient, lasting only as long as the crater takes to collapse[8]. The nature of this fluidization is poorly understood at present and several weakening mechanisms have been suggested. These include thermal softening[9,10], interstitial fluid and melt fluidization[11] and Acoustic Fluidization[12,13]. The weakened and fluidized rock mass rebounds vertically and flows laterally into the transient crater, to form a gravitationally stable, shallower and broader crater with a central uplift at the end of the crater modification stage. The largest of these on Earth form multi-ring or peak ring impact basins, wherein the central uplift dynamically collapses outwards forming a ring of peaks during an extended period of acoustic fluidization/dynamic rock weakening[14,15]. Several marine complex craters also display a crater 'brim', or 'inverted sombrero' morphology[16], wherein concentric normal faults formed during the crater modification stage result in surface deformation beyond the morphological crater rim. This morphology is indicative of impact into a layered target consisting of unconsolidated, fluid-saturated sediments[6,17].

Most preserved craters are partially eroded at Earth's surface, giving depth-limited 'snapshots' of subsurface deformation within these structures[18]. Most other seismically imaged buried impact craters (e.g. Mjolnir[19,20], Chesapeake[17,21], Montagnais[22]) are only imaged with 2D data and have undergone post-modification processes because of tectonics or compaction, preventing a full understanding of structural relationships or observations of sedimentary processes[23–25]. The Silverpit Crater in the North Sea has been partially imaged by 3D seismic and displays many of the characteristics expected for a complex crater[26–28], but the lack of complete seismic coverage and the complexity of the local geology means that a hypervelocity impact origin remains disputed[29]. There are no confirmed craters fully imaged by high-resolution 3D seismic. This limits our understanding of the physical processes involved in crater formation, and the environmental consequences of hypervelocity impact events. Likewise,

[1]School of Energy, Geoscience, Infrastructure and Society, Heriot-Watt University, Edinburgh, UK. [2]TGS, Weybridge, Surrey, UK. [3]Institute for Geophysics & Department of Earth & Planetary Sciences, University of Texas at Austin, Austin, TX, USA. [4]Center for Planetary Systems Habitability, University of Texas at Austin, Austin, TX, USA. [5]Institut für Geo und Umweltnaturwissenschaften, Universität Freiburg, Freiburg im Breisgau, Germany. [6]Lunar and Planetary Laboratory, University of Arizona, Tucson, AZ, USA. [7]Department of Earth Science & Engineering, Imperial College London, London, UK. ✉e-mail: u.nicholson@hw.ac.uk

craters on other planetary bodies in the Solar System can typically only be explored based on their surface morphology or inferred through gravity data.

The Nadir Crater is a proposed hypervelocity impact structure of approximately Cretaceous–Paleogene (K-Pg) boundary age (66 Ma)[30]. The similarity in age of the crater with the 200 km Chicxulub crater in Mexico[31,32], has led to the suggestion that the end-Cretaceous extinction event may have been associated with more than one impact—either breakup of a parent asteroid in near-Earth orbit or as part of a longer-lived (~1–2 My) temporal cluster of impacts[30]. The Nadir Crater has only previously been imaged on two individual 2D seismic profiles, which show characteristics consistent with a complex, mid-sized (≥8.5 km diameter) crater, including a pronounced ≥ 350 m central uplift below the crater floor and large-offset listric normal faults in the annular moat and below the topographic crater rim[30]. The 2D data also allowed the identification of a wide zone of shallow normal faults that extends around two crater radii either side of the crater, interpreted as a damage zone defining the surface 'brim'. However, it is not clear from these limited data whether the crater rim or brim are truly circular (or near circular), and what the spatial variability is of the deformation features both inside and outside of the crater rim. In addition, it is evident from deep seismic artefacts that the seismic processing velocities for the crater in these regional 2D seismic profiles are too low, resulting in poor seismic imaging in the shallow subsurface, particularly around the central uplift.

Although other, epigenetic, mechanisms for crater formation are considered unlikely for the Nadir Crater, uncertainty over a hypervelocity impact origin remains because of the limited data coverage previously published and absence of geological samples[30]. In this paper, we present recently acquired 3D seismic data across the Nadir Crater that allows us to image the surface morphology and subsurface deformation of this pristine crater in exceptional detail. The seismic data cover an area of ~2500 km², (50 km × 50 km), extending >20 km beyond the crater rim in all directions (Fig. 1). These data provide compelling evidence for an impact origin, and a rare opportunity to image the surface and subsurface characteristics of an impact crater in 3D and to test and construct new models of crater development in marine targets.

Geological setting of the Nadir Crater

The Nadir Crater is located offshore Republic of Guinea in West Africa, on the Guinea Plateau, at a water depth of 900 m (Fig. 1). The Guinea Plateau is an extended continental promontory that formed after the breakup of North America and Africa in the Middle-Late Jurassic[33] and then South America and Africa in the Aptian-Albian[34]. The tectonic history and stratigraphic evolution of the Guinea Terrace is constrained by seismic correlation from industry boreholes on the southeast of the Guinea Plateau, where a thick Early Cretaceous to Recent sequence has been drilled[30,34,35]. The stratigraphic sequence consists of a thick package of sedimentary rocks, with up to 8 km of Jurassic to Early Cretaceous carbonates and clastics sitting above volcanic basement. These are overlain by a ~ 2–3 km thick sequence of Aptian to lower Albian clastics that are deformed by normal and transtensional faults. An erosional unconformity separates this sequence from the overlying Albian-Recent sequence that consists predominantly of marine clastic sediments[30,35] deposited in a tectonically quiescent, passive margin.

The crater is located 300 m below the seabed approximately at the K-Pg boundary[30]. The water depth at the time of proposed impact was likely around 800 m, based on seismic analysis of Maastrichtian clinoform heights
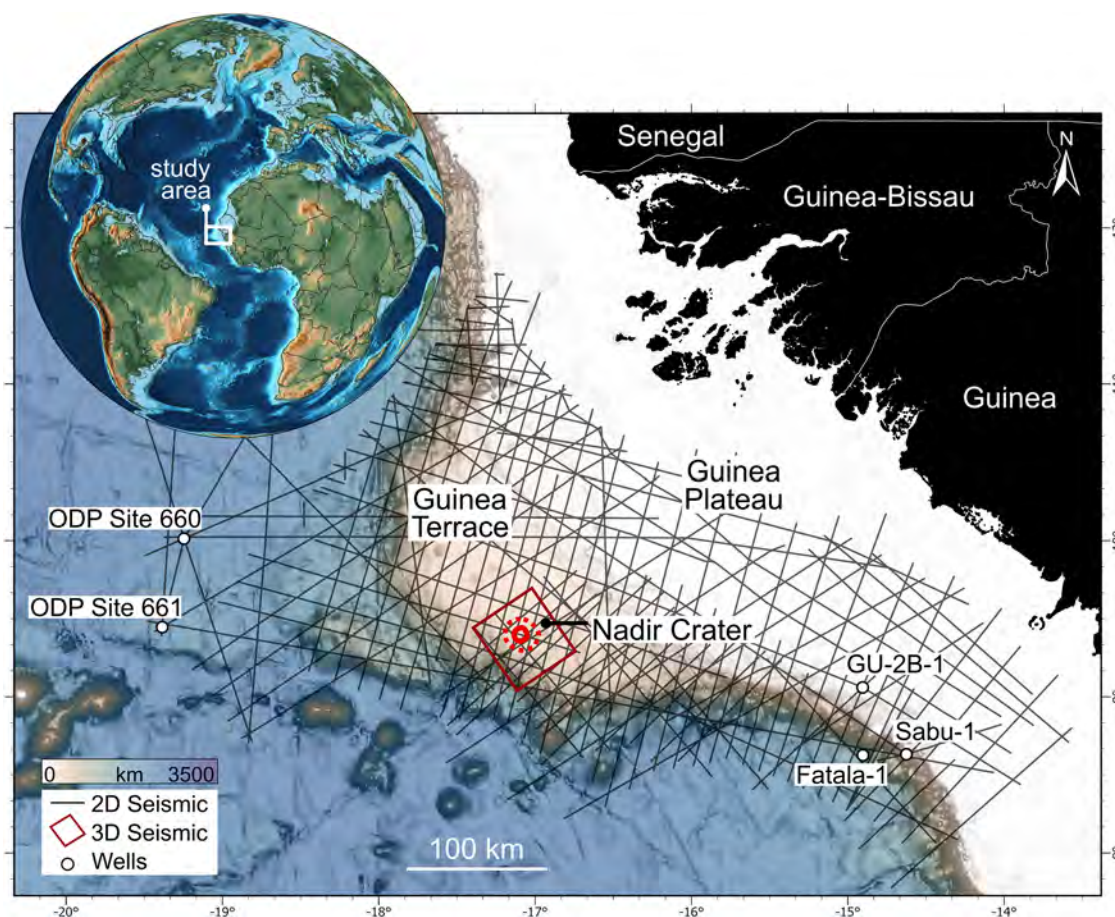
Fig. 1 | Map showing location of Nadir Crater and seismic and well dataset. The MC3D seismic cube used for this study is highlighted in red, with the updated crater outline at the Top Cretaceous horizon defined from 3D (Fig. 2). Seismic data are shown above 15-arc second bathymetry data from GEBCO. The inset map shows the crater location on a paleogeographic reconstruction of the Central Atlantic at 66 Ma. The reconstruction was made using GPlates.
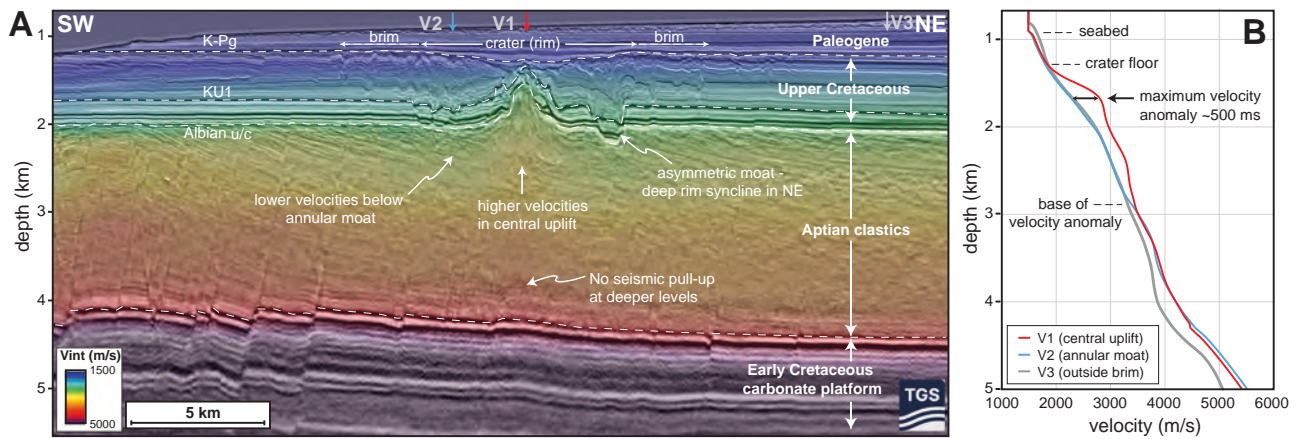
Fig. 2 | Seismic reflection data and velocities across the Nadir Crater. A Seismic section with velocities overlain. Seismic velocities are higher in the central uplift implying a relative reduction in porosity in the uplifted strata as a consequence of the impact. The improved velocity model relative to previous 2D data[30] is also illustrated by the absence of a seismic 'pull-up' artefact at deeper stratigraphic levels. **B** Velocity depth chart showing velocity profiles for three traces, V1, V2 and V3, at different locations with respect to the crater. V1 shows elevated velocities in the central uplift, down to a depth of ~3 km, when compared to V2 and V3. The lower seismic velocities below 3.5 km for V3 is because of the thicker Aptian clastic sequence in that area. An uninterpreted version of the seismic is available in Supplementary Materials (Fig. S1).

and numerical modelling results[30]. The Cretaceous-Recent sequence in which the Nadir Crater is located was deposited on a nearly horizontal seafloor (<1° slope) on the Guinea Terrace, an important consideration for the environmental setting during its formation.

Results

Seismic velocity structure of the crater

Seismic velocities from the pre-stack depth-migrated 3D seismic provide important information on the velocity structure of the crater and target stratigraphy, extending to the base of the stratigraphic sequence (Fig. 2). Velocities increase from around 1500 m/s at the seabed to around 1900 m/s at the top of the Cretaceous (K-Pg). Outside of the crater, and in the annular moat, velocities increase at a consistent rate of around 1000 m/s per km (Fig. 2B). However, relative to stratigraphically equivalent velocities, these are elevated in the central uplift below the crater floor, up to a maximum of 500 m/s higher. Assuming that this velocity effect is primarily due to a reduction in porosity (and corresponding increase in bulk density), this likely corresponds to a 10–15% reduction in porosity in the target stratigraphy in the central uplift[36].

This velocity anomaly extends vertically to around 3 km depth (~1.8 km below the crater floor), below which there is no obvious difference from the surrounding velocity structure. There is also no stratigraphic uplift evident at the bright reflectors at ~4 km depth, confirming that the apparent uplift of strata at and below this depth in older 2D data[30] is a seismic 'pull-up' effect; a processing artefact from the regional 2D velocity model.

Planform morphology of the crater and contemporaneous seabed

The seismic depth map and derived attribute maps of the inferred K-Pg surfaces reveal a near-circular crater, with a rim diameter[37] of ~9.2 km, and an area of ~67 km² (Figs. 3 and 4). The crater planform displays some degree of polygonality, with more linear segments on the northeast and southwest sides. The crater is surrounded by a zone of well-developed concentric features, corresponding to concentric normal faults in the shallow subsurface. The surface (K-Pg) expression of these is used to define the crater brim, which has a diameter of ~22–24 km. The crater surface also displays a clear central peak and terraces within the rim, evident on all three mapped horizons that constitute the expanded K-Pg boundary sequence within the crater (KPg1 through KPg3; Fig. 4). The central peak has a relief of 40 m at the KPg1 horizon, 20 m at the KPg2 horizon and only 10 m at the KPg3 horizon.

The area outside of the topographic crater rim also shows distinctive geomorphological features. There is an arcuate feature evident to the east of the crater (Fig. 3) with a concave-to-the-west geometry that we interpret as a resurge scar[16]. High-variance (discontinuous reflector) facies to the southeast of the crater have a distributive, fan-like morphology expanding away from the crater rim, that we interpret as outwash deposits from the crater. The highest amplitudes at the KPg3 horizon are distributed to the south and west of the crater, possibly indicating the area of thickest ejecta deposits or tsunami-reworked deposits[30].

However, there are also subtle concentric ridges outside of the crater rim, particularly in the north of the seismic volume (Fig. 3). These ridges appear to be formed by irregularities in the extensive underlying chaotic unit that extends far beyond the seismic data, and across much of the Guinea Terrace, previously interpreted as a possible reworked tsunamite layer[30].

Subsurface deformation structures

The structural deformation evident in the subsurface within the ~22–24 km diameter crater brim is more complex in the 3D seismic data than observed from the previous 2D profiles[30] and varies substantially with increasing depth below the K-Pg surface (Fig. 5, Movie S1). At the shallowest continuously mapped surface, KU3, which would have originally been around ~100–150 m below the pre-impact seabed, deformation is dominated by intense folding and faulting in the central uplift, reverse faults within the annular moat, and normal faults in the wider brim. The larger-offset, planar faults to the northeast are linked to underlying normal faults in the Aptian sequence (Figs. 3, 5C–E). Extensional duplexes form southwest and northeast of the crater, indicating lateral transport of material towards the crater (Fig. 5A, B). Deformation at this shallow level is not limited to faulting; complex folds are evident in the shallow stratigraphy, with those in the periphery of the central uplift displaying a tight, isoclinal character, and are even overturned in places. The most intensely folded sequences are associated with thickening of the target stratigraphy towards the crater floor (Fig. 5E).

At deeper stratigraphic levels, from KU2 (originally 500 m below the pre-impact seabed) and below, a well-developed annular moat and central uplift are evident (Fig. 5B). At the KU1 and KU0 levels (~700 and ~900 m below the pre-impact seabed; Fig. 5C and D respectively), deformation is mainly limited to the annular moat and central uplift, with little evidence for deformation up to and beyond the brim. This suggests that the extension dominating the upper levels is accommodated by a detachment fault at a stratigraphic level near the KU1 reflector. The central uplift at these deeper levels is divided into an intensely deformed core and a peripheral zone, the latter being dominated by radial thrust
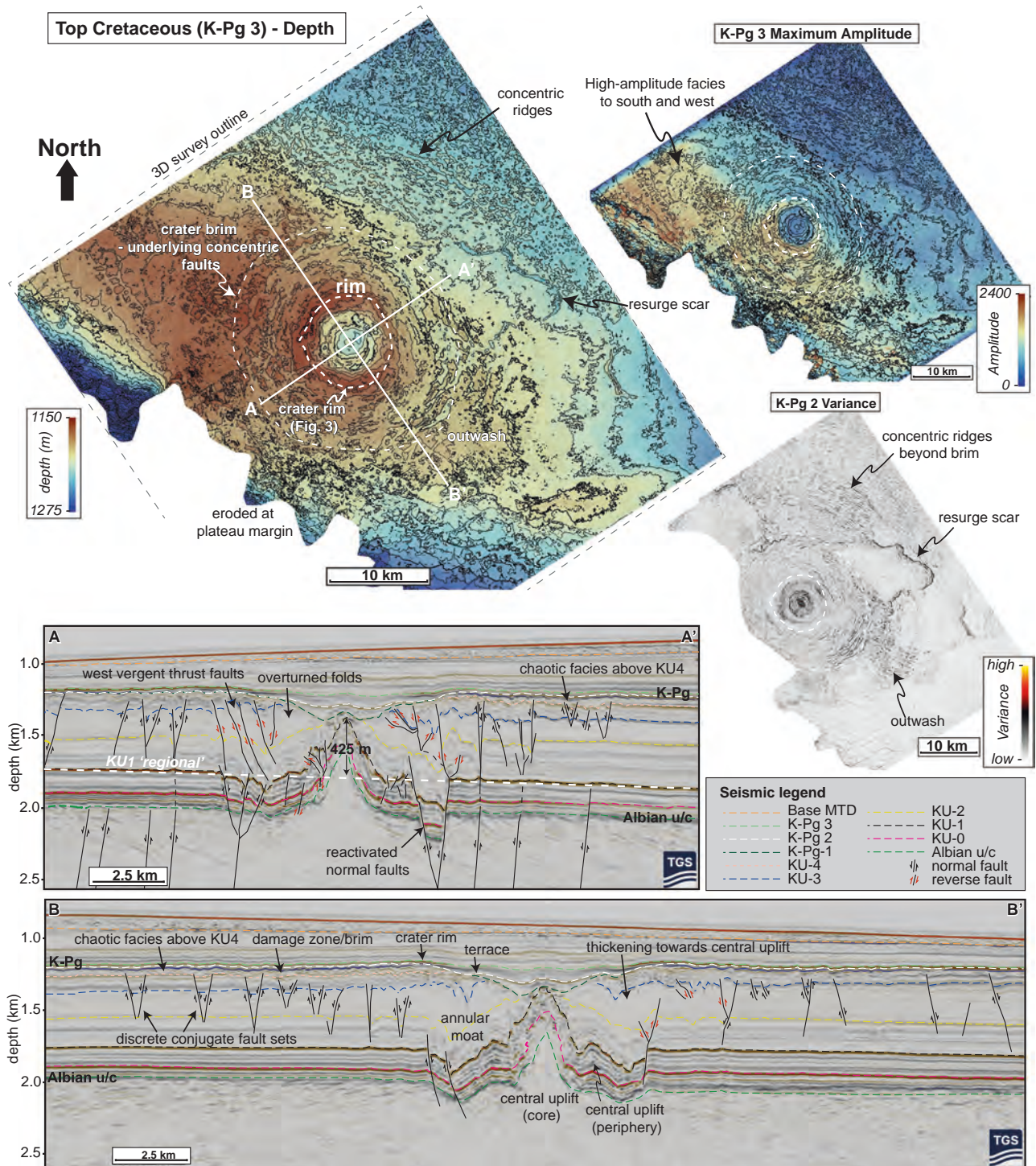
Fig. 3 | K-Pg horizon maps showing the surface expression of the Nadir Crater. The main map shows the top Cretaceous (KPg3) depth surface interpreted from the PSDM seismic cube, with inset maps showing Maximum Amplitude and Variance (reflection continuity) attributes. More detailed maps of the central crater are shown in Fig. 4. The seismic inline (**A–A'**) and crossline (**B–B'**) crosses the centre of the crater. The 3D data reveal more structural complexity around the central uplift, annular moat and deformed crater brim than observed previously on 2D data[30]. The seismic inline (**A–A'**) shows that the deformation pattern is highly asymmetric, with predominantly west-verging thrust faults occurring on both sides of the crater. An uninterpreted version of the seismic is available in Supplementary Materials (Fig. S2).

faults (KU0) and thrust-cored ridges (KU1) (Fig. 5). These radial thrust faults have a concave to the east geometry, with an axis of bilateral symmetry of around 80° (nearly east-west). Vergence on the thrust-cored folds is almost entirely to the west-southwest, showing net transport of material in that direction. Individual faults have a throw of up to 250 m and a total displacement of up to 500 m.

Subsurface deformation also extends to the area outside of the brim at shallow stratigraphic levels. Rectangular fault blocks are present across the entire south and west of the seismic volume, with the dominant structures being southwest-dipping normal faults (Fig. 6). The largest fault blocks are immediately southwest of the crater, with individual blocks of up to 3 km (tangential to the crater) ×2 km (perpendicular to the crater). Tightly spaced
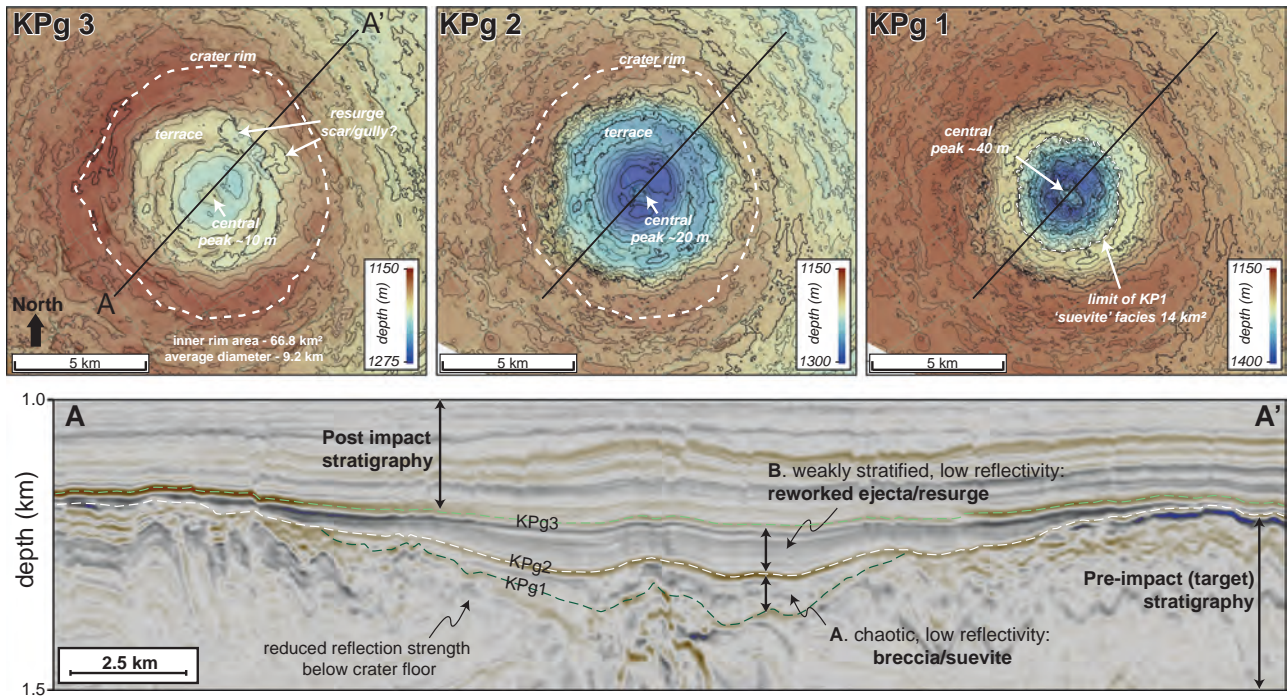
Fig. 4 | Depth maps showing the surface crater morphology at the KPg1, KPg2 and KPg3 horizons. The KPg1 horizon is interpreted as the crater geometry below an in-situ breccia/suevite unit, KPg2 as the crater floor immediately after the crater modification stage, and KPg3 as crater floor after resurge deposition. All three surfaces show a pronounced central uplift, a stepped terrace zone above the rim syncline/annular moat and a well-developed crater rim. The crater depth is greater for KPg1 (~230 m) than for KPg2 (~130 m) or KPg3 (~70 m). Contour interval is 10 m. The inner rim is interpreted at the area of greatest elevation for all three reflections, providing an accurate measure of crater diameter (average 9.2 km) and area (67 km^2). An uninterpreted version of the seismic is available in Supplementary Materials (Fig. S3).

(~500 m) NW-SE trending domino-type normal faults occur to the northwest of the crater with a consistent change of dip direction from southwest to northeast, and a zone of conjugate fault sets in the middle. The region to the east of the crater lacks any substantial deformation, except for 2–3 concentric faults extending up to 5 km beyond the brim, and several concave-up faults that we interpret as 'negative flower structures'. These transtensional strike-slip faults appear to be rooted in older normal faults in the Lower Cretaceous sequence (Fig. 6, B–B').

Discussion
3D seismic evidence for a hypervelocity impact origin

The 3D seismic data provide compelling evidence for a hypervelocity impact origin for the Nadir Crater. The combination of structural and stratigraphic features and velocity data described above allow us to understand the 3D anatomy of this structure in detail. The crater depth to diameter ratio (1:40), central uplift diameter to crater diameter ratio (1:5), stratigraphic uplift to crater diameter ratio (1:22), and the structural characteristics of the stratigraphic uplift and annular moat are all consistent with observations from confirmed impact craters[6,18]. The geomorphic characteristics of the contemporaneous seabed beyond the crater, including the large resurge scar (Fig. 2), are also characteristic of marine craters[16,38]. The increase in seismic velocity and assumed loss of porosity beneath the crater floor is consistent with that observed for sedimentary target and marine target craters such as Mjølnir[20]. The stratigraphy within the crater of a chaotic layer between KPg1 and 2 and a stratified low amplitude layer between KPg2 and 3 (Fig. 4) is consistent with the unsorted suevite deposited during initial crater modification overlain by sorted suevite deposited by the resurge at the marine Chicxulub impact structure[39]. The improved seismic imaging below the crater (Fig. 2) also shows that there are no 'bottom-up' features such as salt diapirism, volcanic vents or other magmatic diapirs that would be consistent with alternative models of circular crater formation[30,40–42].

These data thus provide exceptional support for an impact origin based on geophysical data alone. Most buried impact craters are first identified

morphologically using geophysical data but are not viewed as being confirmed craters formed by hypervelocity impacts without rock samples showing products of high shock pressure unique to impacts[43]. Many geophysical anomalies with circular planform morphologies are non-unique and can be formed by terrestrial processes, and there are multiple examples of such features being wrongly identified as impact structures[43]. However, Nadir is the best global example where 3D imaging provides a complete set of near-diagnostic features which require an impact origin to explain. We consider that the features described above are unique to a hypervelocity impact process, particularly in the context of the Guinea Plateau, where other genetic processes can be definitively ruled out. Therefore, we propose that there can be extraordinary cases where clear imaging of these features using high-resolution seismic data could be viewed as sufficient to classify a structure as an impact crater and that such high-confidence cases merit inclusion in crater databases[4,5,7], particularly for buried craters that cannot be accessed by drilling. Certainly, on other planets, morphology and structural relationships from remote sensing and geophysical data are used to distinguish impacts from other crater-forming processes (e.g. volcanic).

We are aware that identification of shock features in cores is important to ultimately confirm an impact origin when possible. In the case of Nadir, this can potentially be achieved by ocean drilling but for other, more deeply buried, structures, this might not be possible. In such cases, it is important to robustly identify the morphological features described above using geophysical data to consider a hypervelocity impact origin. However, we suggest that the robust identification of such morphological characteristics is only likely to be possible for marine/sedimentary-target impact craters that are rapidly buried after formation, and where the impact stratigraphy and crater fill is sufficiently well preserved and imaged. In light of our observations at Nadir, several candidate marine-target impact craters such as Silverpit[26] or Praia Grande in Brazil[44] could potentially be confidently interpreted as hypervelocity craters with new, high-resolution seismic data that fully cover the craters and immediate surrounding area.
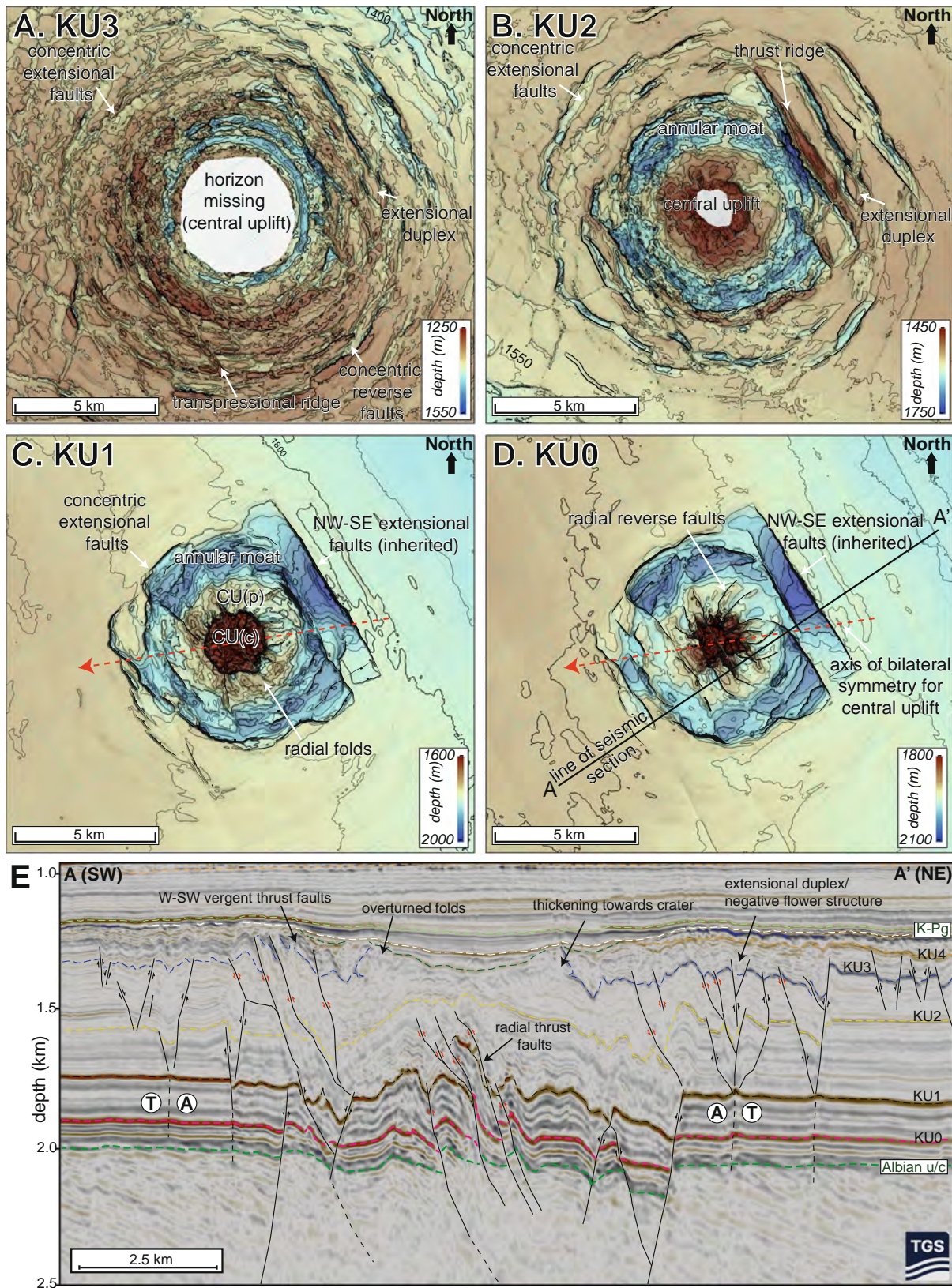
Reconstructing impact angle

Reconstructing impact angle is important to understand the hazard potential of hypervelocity impacts, including quantification of target material vaporized, air blast pressure, thermal radiation, ionospheric disturbance, and tsunami characteristics[3,45,46]. The Nadir Crater is nearly circular in plan view, with the central peak occurring very close to the centre of the crater (Figs. 3, 4). This is consistent with an impact angle greater than 15° above horizontal[18]. However, subsurface deformation, particularly around the central uplift, is not uniform (Figs. 5, 6). The crater is distinctly asymmetric with steeper rim faults and a deeper ring syncline in the

Fig. 5 | Structural characteristics of the Nadir Crater at different stratigraphic levels. A–D Depth maps of mapped Upper Cretaceous reflections (KU0-KU4) highlight the contrast in deformation style between shallower and deeper levels. Shallower levels (KU3, and KU2) display concentric normal faults across a broad area (diameter of ~24 km), with reverse faults limited to areas overlying large normal fault steps in the underlying strata. Deeper levels display nearly concentric faults below the inner rim, which interact with reactivated NW-SE trending Early Cretaceous faults on the NE of the structure. The central uplift is divided into an intensely deformed core (CUc) and a less deformed periphery (CUp), which displays radial folds (KU1) and reverse faults (KU2). These are used to define an axis of bilateral symmetry that we interpret to be parallel to the trajectory of the asteroid during impact (approximately east to west; dashed red arrow in (**C**)). **E** Seismic profile **A–A'** (line location shown in (**D**)) shows the structural characteristics of these radial structures in the periphery, with consistent vergence of thrust faults to the west/south-west, indicating the direction of mass transfer top to the west due to oblique impact. A and T refer to strike-slip movement away from and towards the reader respectively. An uninterpreted version of the seismic is available in Supplementary Materials (Fig. S4).
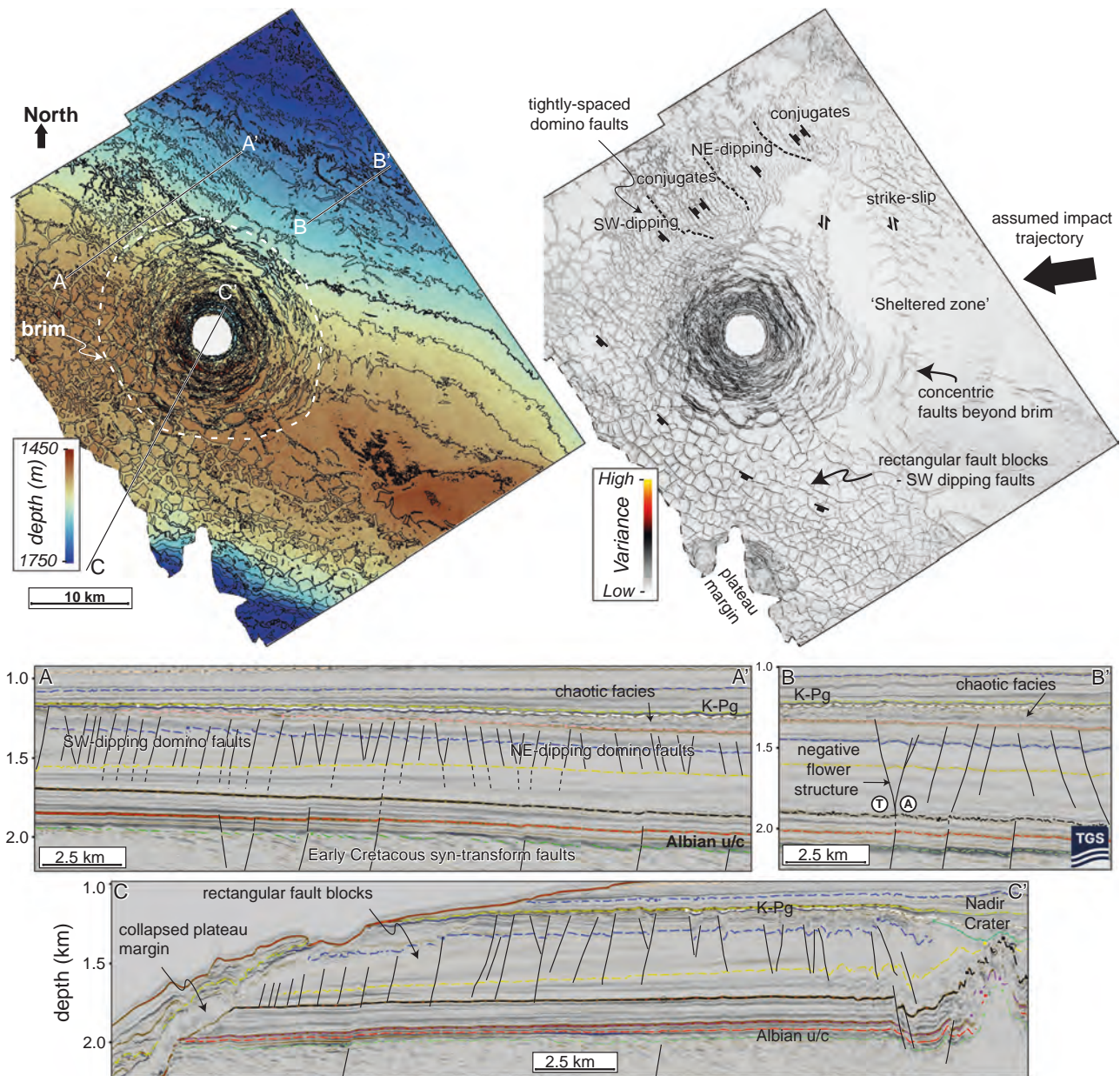
Fig. 6 | Depth and seismic attribute maps of the KU3 horizon, showing deformation patterns in the shallow target stratigraphy outside of the crater brim. Depth map on the top left, seismic variance (reflection continuity) on top right. The location of seismic sections are shown on the depth map. Representative fault types and orientation are shown on the variance map. This surface was approximately ~200 m below the seabed at the time of impact. The brim region is dominated by concentric faults with intense deformation evident outside of the brim in the south and west but largely absent in the 'sheltered zone' to the east, in what is interpreted as the uprange direction. Deformation in the south and west is dominated by rectangular fault blocks, controlled by predominantly SW-dipping normal faults. We interpret these faults to have formed in response to the impact, due to dewatering and volume loss, and the presence of an unconfined plateau margin to the west. Deformation in the north to north-west is characterized by tightly spaced NW-SE trending normal faults, with subsidiary strike-slip elements, oriented perpendicular to the $\sigma 3$ direction induced by lateral (top to the west) transfer of material following the impact. An uninterpreted version of the seismic is available in Supplementary Materials (Fig. S5).

northeast in comparison to the southwest. This is consistent with results of oblique impact experiments[47], impact simulations[48], and observations of confirmed impact craters[49], which show that a deeper annular moat would be expected in the uprange direction. However, inherited and reactivated normal (or transtensional faults) add complexity to the interpretation, as the inherited structural fabric below the Albian unconformity has a strong NW-SE fault orientation[34,35].

We consider that the bilateral symmetry and concave-to-the-east morphology of the radial thrusts provide the best evidence for angle of impact, as the dominant target weakening/acoustic fluidization[12] process in the central uplift means that this area is least susceptible to structural inheritance. Similar curved radial thrusts are observed in a number of other mid-sized impact craters, including Upheaval Dome[50], Spider Crater[51] and Matt Wilson Crater[52]. In these cases, the radial thrusts are characteristic of relatively low-angle impacts, likely under 30°. As with these analogues, the curvature of the imbricated, radial thrusts and the consistent direction of vergence can be used to determine the angle of impact. For Nadir, the thrust faults and related folds are west-southwest verging, which we interpret as the downrange direction. Thus, the impactor that formed the crater likely came from the east-northeast, approximately parallel to the bilateral axis of symmetry of ~80°. The subsurface 'sheltered zone' to the east of the crater (Fig. 6) is consistent with this being the uprange side of a low-angle impact, where shock-related stress would likely be lowest[53]. This can be further tested by future full 3D numerical impact simulations of a marine impact, including more representative physical properties than previously modelled[30]. The impact direction is similar to that of the 200 km K-Pg Chicxulub crater in México, albeit at a lower angle[46].

Beyond the brim: regional subsurface damage zone

The damage zone in sedimentary-target marine craters is typically restricted to an area referred to as the 'brim', that forms because of concentric normal faulting of weak, stratified target material[16,54,55]. This deformation typically extends 1–2 crater diameters from the rim[56], consistent with that which we observe for the Nadir Crater (~1:2.5). However, at Nadir the shallow target stratigraphy also displays extensive structural deformation beyond the brim to the south, west and north, despite the absence of tectonic deformation[35]. This damage zone extends vertically from close to the KU1 horizon to the KPg1 horizon but does not extend into the overlying Paleogene sequence. This strain appears to have been accommodated by a detachment at or near the KU1 horizon. Scientific drill cores from the equivalent sequence on the conjugate South American margin offshore Suriname show that this sequence likely consists of black shales, with a high total organic carbon content[35,57]. Such sediments are known to act as detachment surfaces, or décollement, in tectonic deformation[58].

The fault patterns beyond the brim show pronounced variations in structural style, particularly in the north, west and southwest of the plateau, with respect to the crater. The distribution and character of these contrasting fault groups show that they are clearly linked to the crater itself rather than to pre-existing lithological contrasts or diagenetic processes. We interpret the rectangular fault blocks to the west and southwest to have formed due to a combination of two processes. The first is volume loss due to dewatering and compaction, induced by rapid pore-pressure fluctuations and overpressure generation by seismic shaking during passage of the initial pressure wave. The second contributing factor is the lack of confining stress at the margin of the plateau. This may have resulted in lateral transfer of material to the southwest, as suggested by the dominant west-dipping faults on these structures (Fig. 6B), and initiated collapse of material from the plateau margin[30]. This lateral transfer likely further exacerbates the tendency to generate submarine landslides in such settings, beyond the triggering mechanism represented by seismic shaking. This process of lateral transfer towards the plateau margin also likely explains the geometry and orientation of the domino-type faults to the north of the crater, with the sense of movement (ENE-WSW extension) nearly parallel to the proposed impact trajectory.

The target stratigraphy to the east of the brim doesn't display any evidence of structural deformation, except for two distinct arrays of left-lateral strike-slip faults to the NE of the crater (Fig. 5). This lack of subsurface deformation may be in part due to the greater confining pressures in this area, at a greater distance from the plateau margin. However, we suggest that this area also experiences lower levels of transient stress from the impact itself because of the inferred impact trajectory. We propose therefore that strain beyond the crater primarily occurs downrange and lateral to the crater, with little deformation in the uprange direction in what we refer to as a 'sheltered zone'. This is similar to the 'forbidden zone' concept developed for ejecta distribution from low-angle impacts, where ejecta is not observed directly uprange[47,53,59].

Multi-stage evolution of marine impact craters

Seismic observations and numerical modelling of the Nadir Crater[30] suggest that the transient crater floor and surrounding seafloor was substantially modified in a short time period following the impact. We propose a multi-stage model of crater formation and modification for the Nadir Crater, which is likely to be applicable for marine impact craters generally.

Initial impact excavation resulted in the formation of the transient cavity (Fig. 7A, B). The shock wave, decaying to a seismic wave, would have passed through the brim and wider region during the excavation stage, leading to fracturing, large-scale overpressure generation and seismic shaking across the wider region, far beyond the crater brim (Fig. 7B). This likely occurred in the first few seconds (assuming a P-wave velocity of 1500–2000 m/s) after the impact, although dewatering and fault development likely continued later into the crater modification stage.

This was followed by the transient crater modification, which structural relationships indicate proceeded from inside to out. Formation of the central uplift occurred first, through rebound of the crater floor and inward flow of dynamically weakened/acoustically fluidized target material and faulting. Subsequently, but overlapping in time and starting on the uprange side, inward collapse of the transient crater rim formed the annular moat, or rim syncline, and terraces (Figs. 3, 5, 7C). Away from the central uplift, this stage involved substantial reactivation of pre-existing normal faults, or transtensional faults, especially in the uprange direction.

Crater modification then continued with the inward-lateral (centripetal) transfer of shallow, poorly consolidated target stratigraphy towards the centre of the crater, forming the crater brim (Fig. 7D). The lateral transport of material was associated with both plastic and brittle deformation. Seismic observations show that the shallow stratigraphy is substantially extended in the crater brim area with thickening and reverse faults in the inner part of the annular moat, particularly on the north-east and southwest margins of the crater. Stratigraphic thickening in this sequence occurs due to the space problem resulting from convergent inward flow on a circular structure. Overturned folds are also present, not as part of the ejecta flap (e.g. ref. 18) but within the proximal target stratigraphy, around the annular moat and central uplift periphery. These are proposed to form because of the poorly consolidated nature of the shallow target stratigraphy, rather than from dynamic rock weakening/acoustic fluidization. Strike-slip faults and extensional duplexes also suggest lateral transfer of target material towards the recently evacuated crater during this stage. We note that the reactivated normal faults (Figs. 5E and 7C) form nucleation points for subsequent imbricate thrusts to form underneath the crater rim, likely because of a large step, or displacement, of the detachment surface near the KU1 horizon in the uprange direction. This demonstrates that the normal faults below the crater rim formed prior to the thrust faults that formed as a result of inward flow of material from the crater brim.

The newly formed crater would initially have been around 230 m deep immediately at the end of the crater modification stage, with a prominent central uplift (KPg1 horizon). Although this is shallower than typical impact craters of this size[6], this would have rapidly been infilled by an impact breccia, which are suggested to move in ground-hugging flows during emplacement[31,60,61]. (KPg2) However, in a marine target crater there is a subsequent resurge stage, which results in a rapidly emplaced layer on top of this surface to produce a final, even shallower
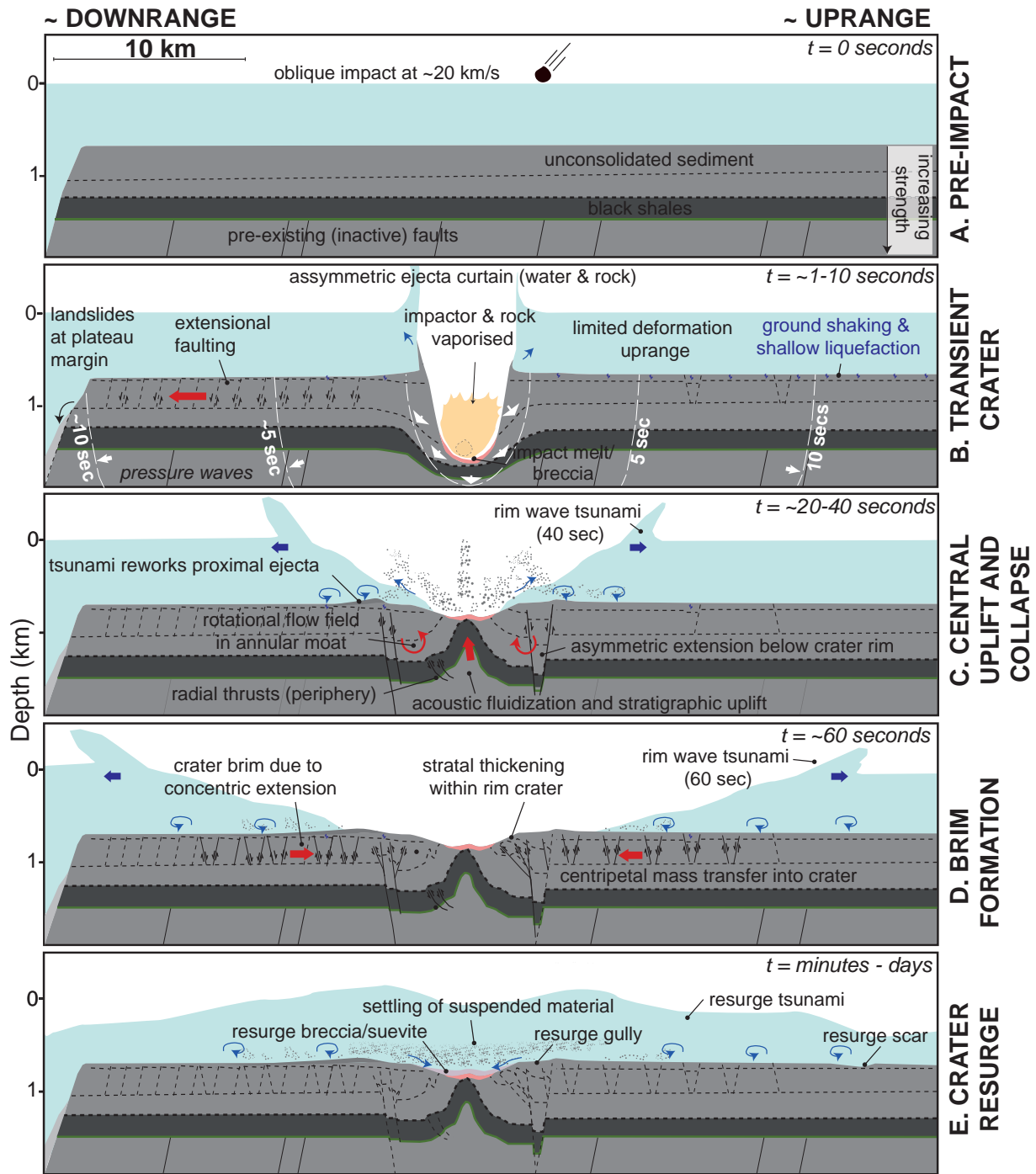
Fig. 7 | Cartoon of multi-stage crater evolution for marine impacts. After the initial impact and formation of the transient crater (**A**, **B**), the crater modification stage is separated into the initial stratigraphic uplift and collapse of the rim and annular moat (**C**), followed by concentric inward flow and formation of the brim (**D**). The surface of the crater continues to be modified by resurge water and subsequent suspension settling (**E**). Some elements are schematic and cannot be accurately represented on a 2D section and there may be some overlap or synchronicity between these stages.

crater floor (KPg3). Evidence of resurge is recorded both as a scar to the east in the 3D volume and as a low-reflectivity layer infilling the crater. At Chicxulub the equivalent resurge deposit is a sorted suevite layer consisting of proximal ejecta and rip-up material that returned to the crater as a turbid resurge flow and then settled on the timescale of hours[31,62].

We also observe possible smaller resurge scars/gullies at the top of the KPg3 horizon, above the terraces (Fig. 3), strengthening the hypothesis that unit B is also part of the late crater modification (resurge) stage rather than post-impact sedimentation within the crater. As noted, similar chaotic seismic facies are observed in 2D seismic data and drillcore at Chicxulub showed this to be a sorted suevite layer that is interpreted to be a resurge deposit[31,39,62].These results show that resurging, transporting both ejecta and additional eroded sediments from the adjacent seabed, results in a suppressed morphology for marine impact craters. In the case of Nadir, the crater depth-to-diameter ratio is reduced from 1:40 to 1:130. This has important implications for the identification of other marine impact craters and for estimating impact size from crater dimensions, particularly depth or crater-fill thickness[30,63].

Marine impact hazards: tsunami-seabed interactions and liquefaction

Following the impact, most of the displaced water moved outward from the impact as a rim-wave tsunami, a product of proximal ejecta landing in the water and the outward movement of the transient cavity in the water layer (Fig. 7B–D)[30]. The high energy of the subsequent resurge event is shown by the presence of the large resurge scar to the east of the crater (Fig. 3). This feature suggests that the returning resurge tsunami amplitude was sufficiently large to interact with the seabed at a distance of ~20 km from the crater rim, even at a likely water depth of ~800 m[30]. This is consistent with numerical models of tsunami heights (depth) for marine-target impacts[30,45]. Resurge gullies have been observed in other marine craters, such as Flynn Creek[16] and Lockne[64] but these are typically narrower and lack the large, arcuate morphology of this feature. Some of the sediment deposited during the resurge was subsequently transported back out of the crater, based on the presence of possible outwash deposits beyond the brim (Fig. 3).

The 3D seismic data also allow us to test the hypothesis that the extensive chaotic layer outside of the crater (Figs. 3, 5), immediately below the contemporaneous crater floor (KPg1) is linked to the impact event[30]. The concentric ridges that form outside of the crater rim are not directly related to underlying structures but appear to be formed within the chaotic unit itself, between the KU 4 and KPg 1 horizons. The distinctive seismic facies are like those observed in mass transport deposits (e.g.[65]), with the concentric ridges in this case inferring lateral (radial) transport of sediment away from the crater. We infer that this unit represents a seismite deposit: rapid dewatering induced by seismic shaking was followed by a phase of outward (with respect to the crater) shear at the seabed caused by the initial train of tsunami waves, leading to buckling and local ramp folding that produced concentric ridges. This facies extends far beyond the seismic survey outline, across much of the Guinea Terrace (see full extent in ref. 30), suggesting that the seismic effects and tsunami waves were sufficiently large to deform and rework the seabed across an area of $\sim 10^5$–10^6 km^2. This may be an important feature for other marine craters and illustrates that shallow hazards associated with liquefaction of water-saturated and uncompacted sediments are a more important factor for subsea infrastructure than has previously been realized.

A natural laboratory for marine impact research

The 3D seismic data across the Nadir Crater provides an exceptional opportunity to test the impact crater hypothesis, develop new models of crater formation in an oblique marine impact and to understand the environmental consequences of such an event. Most other buried impact craters that have been identified in recent decades such as Mjølnir[23,24] and Chesapeake[25] have undergone post-modification processes because of tectonics or compaction, preventing a full understanding of structural relationships or observations of sedimentary processes. Nadir is unique in that it is a pristine crater, relatively unaffected by post-impact processes, as well as being imaged fully in 3D with high-resolution seismic. Nadir therefore provides an ideal natural laboratory for further testing and refining marine impact crater models through further seismic analysis and numerical modelling. High-precision dating of the crater, characterization of subseismic structural and sedimentary features, and final confirmation of an impact origin from shocked minerals, requires the recovery of cores by ocean drilling.

Materials and methods

The MC3D survey in Republic of Guinea was acquired in 2019 by TGS in water depths of 60–4500 m. Acquisition parameters include 12 streamers of 8.025 km length and a separation distance of 150 m. The shot interval was 16.7 m, with a sample rate of 2 ms. Bin dimensions are 6.25 m × 25 m for acquisition and 12.5 m × 12.5 m for processing, with a fold of 80. The record length for the survey is 10,000 ms. Data were processed using a proprietary Pre-Stack Depth Migration (PSDM) sequence (Table S1, Supplementary Materials). Seismic velocities have been tomographically derived to improve imaging around the crater, where velocities vary substantially compared to

the regional trends. Far-field well velocity profiles were used as a starting point for the initial velocity model and the velocities refined using 3D tomography driven by depth-migrated gathers. The long seismic offsets were sufficient to tomographically derive the velocities below the crater floor without passing through the crater itself, to improve confidence in the local velocity anomalies associated with the crater. Seismic interpretation was carried out using Schlumberger Petrel 2020 software, including horizon mapping, structural element mapping, velocity analysis and attribute analysis. Stratigraphic ages were correlated using seismic data from the GU-2B-1 and Sabu-1 wells in the east of the Guinea Plateau. Ages in these wells were derived from industry reports documenting the microfossil assemblages, on cuttings samples (sample interval ~10 m)[35].

Data availability

All data needed to evaluate the conclusions in the paper are present in the paper and/or the Supplementary Materials. Original seismic segy data and well data were provided by TGS and the Republic of Guinea under a confidentiality agreement and remain the property of these organizations. For enquiries about data access, please contact TGS at https://www.tgs.com/seismic. Seismic surfaces displayed in the manuscript can be accessed through the National Geoscience Data Centre, doi:10.5285/662fc0c4-200b-462d-bd17-46354967692d.

References

1. Alvarez, L. W., Alvarez, W., Asaro, F. & Michel, H. V. Extraterrestrial cause for the Cretaceous-Tertiary extinction. *Science* **208**, 1095–1108 (1980).
2. Rumpf, C. M., Lewis, H. G. & Atkinson, P. M. Population vulnerability models for asteroid impact risk assessment. *Meteorit. Planet. Sci.* **52**, 1082–1102 (2017).
3. Shuvalov, V. et al. Asteroid Apophis: evaluating the impact hazards of such bodies. *Sol. Syst. Res.* **51**, 44–58 (2017).
4. Schmieder, M. & Kring, D. A. Earth's impact events through geologic time: a list of recommended ages for terrestrial impact structures and deposits. *Astrobiology* **20**, 91–141 (2020).
5. Gottwald, M., Kenkmann, T. & Reimold, W. U. *Terrestrial impact structures: the TanDEM-X atlas*. (Verlag Dr. Friedrich Pfeil, 2020).
6. Kenkmann, T. The terrestrial impact crater record: a statistical analysis of morphologies, structures, ages, lithologies, and more. *Meteorit. Planet. Sci.* **56**, 1024–1070 (2021).
7. Osinski, G. R. et al. Impact Earth: a review of the terrestrial impact record. *Earth Sci. Rev.* **232**, 104112 (2022).
8. Melosh, H. & Ivanov, B. Impact crater collapse. *Annu. Rev. Earth Planet. Sci.* **27**, 385–415 (1999).
9. O'Keefe, J. D. & Ahrens, T. J. Planetary cratering mechanics. *J. Geophys. Res.: Planets* **98**, 17011–17028 (1993).
10. O'Keefe, J. D. & Ahrens, T. J. Complex craters: relationship of stratigraphy and rings to impact conditions. *J. Geophys. Res. Planets* **104**, 27091–27104 (1999).
11. Spray, J. G. & Thompson, L. M. Friction melt distribution in a multi-ring impact basin. *Nature* **373**, 130–132 (1995).
12. Melosh, H. J. Acoustic fluidization: a new geologic process? *J. Geophys. Res. Solid Earth* **84**, 7513–7520 (1979).
13. Melosh, H. J. *Impact cratering: a geologic process*. (New York, Oxford University Press, Oxford: Clarendon Press, 1989).
14. Morgan, J. V. et al. The formation of peak rings in large impact craters. *Science* **354**, 878–882 (2016).
15. Riller, U. et al. Rock fluidization during peak-ring formation of large impact structures. *Nature* **562**, 511–518 (2018).
16. Adrian, D. R., King, D. T. Jr & Ormö, J. Resurge gullies and "inverted sombrero" morphology, Flynn Creek impact structure, Tennessee. *Meteorit. Planet. Sci.* **54**, 2758–2768 (2019).

17. Poag, C. W. Structural outer rim of Chesapeake Bay impact crater: seismic and bore hole evidence. *Meteorit. Planet. Sci.* **31**, 218–226 (1996).

18. Kenkmann, T., Poelchau, M. H. & Wulf, G. Structural geology of impact craters. *J. Struct. Geol.* **62**, 156–182 (2014).

19. Gudlaugsson, S. T. Large impact crater in the Barents Sea. *Geology* **21**, 291–294 (1993).

20. Tsikalas, F., Gudlaugsson, S. T., Eldholm, O. & Faleide, J. I. Integrated geophysical analysis supporting the impact origin of the Mjølnir structure, Barents Sea. *Tectonophysics* **289**, 257–280 (1998).

21. Poag, C. W. et al. Deep Sea Drilling Project Site 612 bolide event: new evidence of a late Eocene impact-wave deposit and a possible impact site, US east coast. *Geology* **20**, 771–774 (1992).

22. Jansa, L. F., Pe-Piper, G., Robertson, P. B. & Friedenreich, O. Montagnais: a submarine impact structure on the Scotian Shelf, eastern Canada. *Geol. Soc. Am. Bull.* **101**, 450–463 (1989).

23. Corseri, R., Gac, S., Faleide, J. I. & Planke, S. The tectonized central peak of the Mjølnir Impact Crater, Barents Sea. *J. Struct. Geol.* **131**, 103953 (2020).

24. Tsikalas, F. & Faleide, J. I. Post-impact structural crater modification due to sediment loading: an overlooked process. *Meteorit. Planet. Sci.* **42**, 2013–2029 (2007).

25. Kulpecz, A. A. et al. Post-impact deposition in the Chesapeake Bay impact structure: variations in eustasy, compaction, sediment supply, and passive-aggressive tectonism. The ICDP-USGS deep drilling project in the Chesapeake Bay impact structure: results from the Eyreville core holes. *Geol. Soc. Am. Spec. Pap.* **458**, 811–837 (2009).

26. Stewart, S. A. & Allen, P. J. A 20-km-diameter multi-ringed impact structure in the North Sea. *Nature* **418**, 520–523 (2002).

27. Wall, M. L., Cartwright, J. & Davies, R. J. An Eocene age for the proposed Silverpit impact crater. *J. Geol. Soc.* **165**, 781–794 (2008).

28. Stewart, S. & Allen, P. 3D seismic reflection mapping of the Silverpit multi-ringed crater, North Sea. *Geol. Soc. Am. Bull.* **117**, 354–368 (2005).

29. Underhill, J. R. An alternative origin for the 'Silverpit crater. *Nature* **428**, 1–2 (2004).

30. Nicholson, U., Bray, V. J., Gulick, S. P. & Aduomahor, B. The Nadir Crater offshore West Africa: a candidate Cretaceous-Paleogene impact structure. *Sci. Adv.* **8**, eabn3096 (2022).

31. Gulick, S. P. et al. The first day of the Cenozoic. *Proc. Natl Acad. Sci.* **116**, 19342–19351 (2019).

32. Goderis, S. et al. Globally distributed iridium layer preserved within the Chicxulub impact structure. *Sci. Adv.* **7**, eabe3647 (2021).

33. Manspeizer, W. Triassic–Jurassic rifting and opening of the Atlantic: an overview. *Dev. Geotecton.* **22**, 41–79 (1988).

34. Olyphant, J. R., Johnson, R. A. & Hughes, A. N. Evolution of the Southern Guinea Plateau: implications on Guinea-Demerara Plateau formation using insights from seismic, subsidence, and gravity data. *Tectonophysics* **717**, 358–371 (2017).

35. Aduomahor, B., Wagner, T., Duarte, D., Dunkley-Jones, T. & Nicholson, U. Seismic stratigraphy of the Guinea Plateau before, during and after the opening of the Equatorial Atlantic Gateway. *arXiv preprint doi.org/10.31223/X5PH49* (2024). https://doi.org/10.31223/X5PH49.

36. Lee, M. W. Modified Biot-Gassmann theory for calculating elastic velocities for unconsolidated and consolidated sediments. *Mar. Geophys. Res.* **23**, 403–412 (2002).

37. Turtle, E. et al. Impact structures: what does crater diameter mean. *Large Meteor. Impacts III* **384**, 1–24 (2005).

38. Ormö, J. & Lindström, M. When a cosmic impact strikes the sea bed. *Geol. Mag.* **137**, 67–80 (2000).

39. Christeson, G., Morgan, J. & Gulick, S. Mapping the Chicxulub impact stratigraphy and peak ring using drilling and seismic data. *J. Geophys. Res.: Planets* **126**, e2021JE006938 (2021).

40. Stewart, S. Seismic interpretation of circular geological structures. *Pet. Geosci.* **5**, 273–285 (1999).

41. Nicholson, U. & Stow, D. Erosion and deposition beneath the Subantarctic Front since the Early Oligocene. *Sci. Rep.* **9**, 1–9 (2019).

42. Polonia, A. et al. Lower plate serpentinite diapirism in the Calabrian Arc subduction complex. *Nat. Commun.* **8**, 2172 (2017).

43. French, B. M. & Koeberl, C. The convincing identification of terrestrial meteorite impact structures: what works, what doesn't, and why. *Earth Sci. Rev.* **98**, 123–170 (2010).

44. Correia, G. A., de Menezes, J. C., Bueno, G. V. & Marques, E. J. J. in *Proc. 9th International Congress of the Brazilian Geophysical Society*. cp-160-00221 (European Association of Geoscientists & Engineers).

45. Wünnemann, K., Collins, G. & Weiss, R. Impact of a cosmic body into Earth's ocean and the generation of large tsunami waves: insight from numerical modeling. *Rev.Geophys.* **48**, RG4006 (2010).

46. Collins, G. S. et al. A steeply-inclined trajectory for the Chicxulub impact. *Nat. Commun.* **11**, 1–10 (2020).

47. Gault, D. E. & Wedekind, J. A. Experimental studies of oblique impact. *Proc. Lunar and Planetary Science Conference*, *9th, Houston, Tex., March 13-17, 1978, Proceedings.* Vol. 3. (A79-39253 16-91) 3843–3875 (New York, Pergamon Press, Inc., 1978).

48. Davison, T. & Collins, G. Complex crater formation by oblique impacts on the Earth and Moon. *Geophys. Res. Lett.* **49**, e2022GL101117 (2022).

49. Schultz, P. H. & Anderson, R. R. Asymmetry of the Manson impact structure: evidence for impact angle and direction. *Geol. Soc. Am. Spec. Pap.* **302**, 397–417 (1996).

50. Kenkmann, T., Jahn, A., Scherler, D. & Ivanov, B. A. Structure and formation of a central uplift: a case study at the Upheaval Dome impact crater, Utah. *Geol. Soc. Am. Spec. Pap.* **384**, 85–115 (2005).

51. Shoemaker, E. & Shoemaker, C. Impact structures of western Australia. *Meteoritics* **20**, 754 (1985).

52. Kenkmann, T. & Poelchau, M. H. Low-angle collision with Earth: the elliptical impact crater Matt Wilson, Northern Territory, Australia. *Geology* **37**, 459–462 (2009).

53. Pierazzo, E. & Melosh, H. Understanding oblique impacts from experiments, observations, and modeling. *Annu. Rev. Earth Planet. Sci.* **28**, 141–167 (2000).

54. Horton, J. W. Jr, Ormö, J., Powars, D. S. & Gohn, G. S. Chesapeake Bay impact structure: morphology, crater fill, and relevance for impact structures on Mars. *Meteorit. Planet. Sci.* **41**, 1613–1624 (2006).

55. Gohn, G. et al. Deep drilling into the Chesapeake Bay impact structure. *science* **320**, 1740–1745 (2008).

56. Poag, C. W. et al. Residual Effects of Chesapeake Bay Impact. *The Chesapeake Bay Crater: Geology and Geophysics of a Late Eocene Submarine Impact Structure*, 433–446 (Springer, 2004).

57. Trabucho Alexandre, J. et al. The mid-Cretaceous North Atlantic nutrient trap: black shales and OAEs. *Paleoceanography* **25** (2010).

58. Morley, C. et al. Review of major shale-dominated detachment and thrust characteristics in the diagenetic zone: part I, meso-and macro-scopic scale. *Earth Sci. Rev.* **173**, 168–228 (2017).

59. Herrick, R. R. & Hessen, K. K. The planforms of low-angle impact craters in the northern hemisphere of Mars. *Meteorit. Planet. Sci.* **41**, 1483–1495 (2006).

60. Siegert, S., Branney, M. J. & Hecht, L. Density current origin of a melt-bearing impact ejecta blanket (Ries suevite, Germany). *Geology* **45**, 855–858 (2017).

61. McCall, N. et al. Understanding the Ries impact structure subsurface from high-resolution seismic data. *Geology* **52**, 39–44 (2023).

62. Kaskes, P. et al. Formation of the crater suevite sequence from the Chicxulub peak ring: a petrographic, geochemical, and sedimentological characterization. *GSA Bull.* **134**, 895–927 (2022).

63. Davison, T. & Collins, G. S. The effect of the oceans on the terrestrial crater size-frequency distribution: Insight from numerical modeling. *Meteorit. Planet. Sci.* **42**, 1915–1927 (2007).

64. Dalwigk, I.von & Ormö, J. Formation of resurge gullies at impacts at sea: the Lockne crater, Sweden. *Meteorit. Planet. Sci.* **36**, 359–369 (2001).

65. Nicholson, U., Libby, S., Tappin, D. R. & McCarthy, D. The Subantarctic Front as a sedimentary conveyor belt for tsunamigenic submarine landslides. *Mar. Geol.* **424**, 106161 (2020).

Author contributions

U.N. was responsible for conceptualization of the key research idea, led the research grant for funding specific to this project, was the main interpreter of the data, wrote the original draft and carried out subsequent editing. W.P. also conceptualized the idea and interpreted the data and contributed to reviewing and editing the manuscript. S.G. contributed to funding acquisition, data interpretation and reviewing and editing the manuscript. T.K., V.B., D.D. and G.C. all contributed to the data interpretation and reviewing and editing of the manuscript.

Competing interests

The authors declare no competing interests.

Additional information

Supplementary information The online version contains supplementary material available at https://doi.org/10.1038/s43247-024-01700-4.

Correspondence and requests for materials should be addressed to Uisdean Nicholson.

Peer review information *Communications Earth & Environment* thanks Romain Corseri, Luca Gasperini and Marc Biren for their contribution to the peer review of this work. Primary Handling Editors: Kim Welford and Joe Aslin. A peer review file is available.

Reprints and permissions information is available at http://www.nature.com/reprints